LES of wind environments in urban residential areas based on an inflow turbulence generating approach

Lian Shen[1], Yan Han[*1], C.S. Cai[2], Guochao Dong[1],
Jianren Zhang[1] and Peng Hu[1]

[1]*School of Civil Engineering and Architecture, Changsha University of Science & Technology, Changsha, China, 410004*
[2]*Department of Civil and Environmental Engineering, Louisiana State University, Baton Rouge, USA, LA 70803*

Abstract. Wind environment in urban residential areas is an important index to consider when evaluating the living environment. However, due to the complexity of the flow field in residential areas, it is difficult to specify the correct inflow boundary conditions in the large eddy simulation (LES). In this paper, the weighted amplitude wave superposition (WAWS) is adopted to simulate the fluctuating velocity data, which satisfies the desired target wind field. The fluctuating velocity data are given to the inlet boundary of the LES by developing an UDF script, which is implemented into the FLUENT. Then, two numerical models ─ the empty numerical wind tunnel model and the numerical wind tunnel model with spires and roughness elements are established based on the wind tunnel experiment to verify the present method. Finally, the turbulence generation approach presented in this paper is used to carry out a numerical simulation on the wind environment in an urban residential area in Lisbon. The computational results are compared with the wind tunnel experimental data, showing that the numerical results in the LES have a good agreement with the experimental results, and the simulated flow field with the inlet fluctuations can generate a reasonable turbulent wind field. It also shows that strong wind velocities and turbulent kinetic energy occur at the passageways, which may affect the comfort of people in the residential neighborhood, and the small wind velocities and vortexes appear at the leeward corners of buildings, which may affect the spreading of the pollutants.

Keywords: large eddy simulation; wind environment; WAWS; fluctuating wind field

1. Introduction

With the rapid development of computer technology and the computational fluid dynamics (CFD) theory, CFD technology has been widely used as an analysis method for wind engineering, sometimes in lieu of wind tunnel experiments. The Navier-Stokes equations govern the flow of wind fields, and various numerical methods have been devised to obtain the solution of the equations. At present, the mainstream turbulence models are the Reynolds Averaged Navier-Stokes formulations (RANS) and the Large Eddy Simulation (LES). In terms of the numerical simulation

---

∗Corresponding author, Associate Professor, E-mail: ce_hanyan@163.com

on wind environment for urban residential areas, there is a consensus on the fact that the LES is more accurate than the RANS (Gousseau, Blocken *et al*. 2012). Compared with the RANS, the LES could demonstrate more detailed flow fluctuating information. The LES resolves large-scale unsteady motions and requires only small-scale models. Therefore, by using LES, wind field properties such as the fluctuating information at urban residential scales, which are primarily due to large-scale motions, can be directly solved. Therefore, LES is favored in many cases and is used by many researchers (Jiang and Miao 2004).

Different scales of air movement affect the wind environment, which is an important part of urban atmospheric microenvironments in an urban residential area (Britter and Hanna 2003). It is quite complicated due to the thermal convection caused by the temperature difference of the flow field in the horizontal direction, the whirlpool interaction between the surface of the urban boundary layer and the urban canopy in the vertical direction, and the local turbulence caused by architectural complex, trees, as well as billboards (Cui, Zhang *et al*. 2013). When simulating wind environment in urban residential areas using LES, a crucial issue is imposing the correct inflow turbulence on the inlet boundary. The incoming flow field should have the targeted spatial and temporal characteristics that reflect the actual wind field. The influence of inflow turbulence on the LES had been presented by Tominaga, Mochida *et al*. (2008). It has been confirmed that the inflow turbulence is extremely important for the LES.

There have been many attempts to deal with the inflow boundary conditions in the past two decades (Kondo, Murakami *et al*. 1997, Smirnov, Shi *et al*. 2001, Hanna, Tehranian *et al*. 2002, Tamura 2000, Noda and Nakayama 2003, Huang, Li *et al*. 2010, Tabor and Baha-Ahmadi 2009, Wang, Yu *et al*. 2015, Liu, Ishihara *et al*. 2016a, b). Those concerned research approaches can be generally classified into three kinds. The first one is the "precursor simulation" method in which the targeted wind field is simulated in advance in a pre-simulation zone and then assigned to the inflow boundary of the major simulation zone. This method has been widely used for generating inflow fluctuations (Keating *et al*. 2004, Chung and Sung 1997, Tamura, Tsubokura *et al*. 2003, Jiang and Miao 2012). The turbulence generated by this method has a good temporal and spatial correlation and a correct energy spectrum, but the disadvantage of this method lies in the large consumption of storage space and time to generate the matched database. The second one is the vortex method (Mathey, Cokljat *et al*. 2006) in which a random 2D vortex is used at the inlet to add perturbations on a specified mean velocity profile. This method can generate a fluctuating wind field, which has a good spatial correlation and turbulence energy. However, the target spectrum and statistical characteristics of the inflow turbulence are not explicitly expressed in its generating procedure. The third one is the synthetic method in which the main strategy is to superimpose the mean quantities with synthetic randomness (Maruyama and Morikawa 1999, Huang, Li *et al*. 2010, Hanna, Tehranian *et al*. 2002, Hemon and Santiet 2007, Xie and Castro 2008). This method was first proposed by Kraichnan (1970), and developed by Iwatani (1982) and Maruyama (1994). Kondo, Murakami *et al*. (1997) modified this method, in which the power spectral density and the cross-spectral density obtained from FFT analyses of the time series of wind velocity fluctuations were used to construct the trigonometric series with the Gaussian random coefficients. In this method the target power spectral density and the root mean square (RMS) value of the fluctuating wind velocity can be imposed in the generation procedure for a random flow field, and thus the target characteristics can be guaranteed. However, the divergence-free condition cannot be ensured for the generated flow field. Smirnov, Shi *et al*. (2001) proposed a method to generate an isotropic divergence-free fluctuating velocity field with the target turbulence length and time scales. In Smirnov's method, the turbulence length scale and the

time scale were incorporated into the basic model proposed by Kraichnan (1970). Meanwhile, the inhomogeneous and anisotropic turbulence characteristics were realized by a scaling and orthogonal transformation of the resulted flow field with a given anisotropic velocity correlation tensor. However, the disadvantage of Smirnov's method is that the power spectrum of the generated turbulent flow field only follows the Gaussian spectral model. However, for the Gaussian spectral model, the dissipation subrange may be neglected in the turbulent flow field. Huang, Li *et al*. (2012) extended Smirnov's method, in which the divergence-free condition was satisfied, and the generation procedure is independent for each point, which is very suitable for conducting parallel computations. Castro and Paz (2012) included a dimensionless time scale parameter to establish the temporal correlation of the synthetic velocity fluctuations. The major advantage of the spectral method is to yield an "essentially" divergence-free turbulent flow field. Recently, Yu and Bai (2014) introduced a vector potential field into Smirnov's method (2001) and generated a strictly divergence-free turbulent flow field. Yan and Li (2015) comprehensively evaluated the performances of four inflow turbulence methods used to simulate wind flows in the atmospheric boundary layer for LES of wind loadings on a tall building. However, to the best of the authors' knowledge, comprehensive applications of these methods in the simulation of the wind environment in urban residential areas had rarely been conducted before.

An efficient technique to generate the inflow turbulence for LES based on the weighted amplitude wave superposition (WAWS) method, which belongs to the third category as mentioned above, is provided in this paper. The generated turbulent flow field in the LES can satisfy the Kaimal model or any desired spectrum, and the spatial correlation and power spectrum density function can agree well with the given target spectrum. Meanwhile, a UDF script is implemented into the FLUENT to assign the generated turbulent inflow velocity data to the inlet boundary of the LES. Then, the two numerical models ─ the empty numerical wind tunnel model and the numerical wind tunnel model with spires and roughness elements are established based on the wind tunnel experiment to verify the presented approach. The computational results of the flow field in the empty numerical wind tunnel model are compared with the wind tunnel experimental data, and the accuracy of the presented approach is confirmed. Meanwhile, the computational results of the flow field in the numerical wind tunnel model with the spires and roughness elements are compared with those of the flow field in the empty numerical wind tunnel, and the effectiveness of the presented approach is verified. Finally, the turbulence generation approach introduced in this paper is used to carry out a numerical simulation on the wind environment in an urban residential area in Lisbon, and the wind environment is assessed based on the simulated results.

2. Methodology of numerical simulations

2.1 LES modeling

LES has been become an important tool for the study of turbulent flows in urban residential areas. The basic premise in the LES is that the largest eddies contain most of the energy and are responsible for most of the transport of momentum and scalars. The scales smaller than the grid-filter size are eliminated. The governing equations used for the LES are derived from the classical time-dependent filtered Navier-Stokes (N-S) equations

$$\frac{\partial \overline{u}_i}{\partial x_i} = 0 \tag{1}$$

$$\frac{\partial \overline{u}_i}{\partial t} + \frac{\partial \overline{u}_i \overline{u}_j}{\partial x_j} = -\frac{1}{\rho}\frac{\partial \overline{p}}{\partial x_i} + \frac{\partial}{\partial x_j}[(v\frac{\partial \overline{u}_i}{\partial x_j} + \frac{\partial \overline{u}_j}{\partial x_i}) + \tau_{ij}] \tag{2}$$

where $\overline{u}$ and $\overline{p}$ are the filtered velocity and pressure, respectively, v is the kinematic viscosity; and τ_{ij} is the sub-grid scale (SGS) stress and can be expressed as

$$\tau_{ij} = \overline{u_i u_j} - \overline{u}_i \overline{u}_j \tag{3}$$

The SGS stress τ_{ij} is computed based on the turbulent eddy viscosity, μ_t. In order to close the N-S equations, τ_{ij} can be expressed according to Boussinesq's approximation

$$\tau_{ij} - \frac{1}{3}\tau_{kk}\delta_{ij} = -2\mu_t \overline{S}_{ij} \tag{4}$$

where μ_t is the subgrid-scale eddy-viscosity. The isotropic part of the subgrid-scale stresses, τ_{kk}, is not modeled, but it is added to the filtered static pressure term. $\overline{S}_{ij}$ is the rate-of-strain tensor for the resolved scale defined by

$$\overline{S}_{ij} = \frac{1}{2}(\frac{\partial \overline{u}_i}{\partial x_j} + \frac{\partial \overline{u}_j}{\partial x_i}) \tag{5}$$

In the Smagorinsky-Lilly model, the eddy-viscosity is modeled by

$$\mu_t = \rho L_S^2 |\overline{S}| \tag{6}$$

where L_S is the mixing length for subgrid scales and $\overline{S} = (2\overline{S}_{ij}\overline{S}_{ij})^{1/2}$, and L_S is computed using

$$L_S = \min(kd, C_S\Delta) \tag{7}$$

where k is the von Kármán constant, d is the distance to the closest wall, C_S is the Smagorinsky constant defined by Lilly and is 0.23, and Δ is the local grid scale. In the ANSYS FLUENT, Δ is computed according to the volume of the computational cell using

$$\Delta = V^{1/3} \tag{8}$$

In this paper, the SGS model by Smagorinsky-Lilly (Fluent, Education version, V15.0) is used to account for the turbulence, and the discretization schemes and solution technique are summarized in Table 1.

Table 1 Discretization schemes and solution technique

Parameter	Type
Time discretization	Second order implicit
Pressure discretization	Second order upwind
Momentum discretization	Bounded central difference
Pressure-velocity coupling	Pressure-implicit with splitting operators (PISO)
Under relaxation factors	0.3 for the pressure and 0.7 for the momentum

2.2 Turbulent inflow velocity data generation

WAWS is a classical method to generate the turbulence, and it is widely used by many researchers (Shinozuka, Yun *et al*. 1990, Deodatis 1996, Mann 1998, Di Paola 1998, Ding, Zhu *et al*. 2011). In this study, Deodatis's (1996) method is adopted to generate the turbulent inflow velocity data based on our previous study (Chen, Han *et al*. 2009). To simulate the stationary stochastic process $f_j^0(t)$ (j=1, 2, … , n), the cross-spectral density matrix, $S^0(\omega)$, must be decomposed into the following formulation at first

$$S^0(\omega) = H(\omega)H^{T^*}(\omega) \tag{9}$$

where the superscript T = transpose of a matrix; and ω is the frequency. This decomposition is performed by Cholesky's method, and the lower triangular matrix $H(\omega)$ is given by

$$H(\omega) = \begin{bmatrix} H_{11}(\omega) & 0 & ... & 0 \\ H_{21}(\omega) & H_{22}(\omega) & ... & 0 \\ ... & ... & ... & ... \\ H_{n1}(\omega) & H_{n2}(\omega) & ... & H_{nn}(\omega) \end{bmatrix} \tag{10}$$

The cross-correlation matrix $S^0(\omega)$ is defined as

$$S^0(\omega) = \begin{bmatrix} S_{11}^0(\omega) & S_{12}^0(\omega) & ... & S_{1n}^0(\omega) \\ S_{21}^0(\omega) & S_{22}^0(\omega) & ... & S_{2n}^0(\omega) \\ ... & ... & ... & ... \\ S_{n1}^0(\omega) & S_{n2}^0(\omega) & ... & S_{nn}^0(\omega) \end{bmatrix} \tag{11}$$

where $S_{jj}^0(\omega)$ (j=1, 2, 3, …, n) is the power spectral density (PSD) functions of the components of the process; and $S_{jk}^0(\omega)$ (j=1, 2, 3, … , n; k=1, 2, 3, … , n. $j{\neq}k$) is the cross-spectral density function. While the PSD function is a real and non-negative function of ω, the cross-spectral density function is a complex function of ω.

When *N* approaches infinity, and $f_j(t)$ generated by $S^0(\omega)$ can be formulated as

$$f_j(t) = \sqrt{2} \sum_{m=1}^{j} \sum_{l=1}^{N} |H_{jm}(\omega_{ml})| \sqrt{\Delta\omega} \cdot \cos[\omega_{ml}t - \theta_{jm}(\omega_{ml}) + \phi_{ml}] \tag{12}$$

where $\theta_{jk}(\omega) = \tan^{-1} \left\{ \dfrac{I_m[H_{jk}(\omega)]}{R_e[H_{jk}(\omega)]} \right\}$; *j*=1, 2, 3..., *n*; *Im* and *Re* are the imaginary and real parts,

respectively; $\omega_{ml} = (l-1).\Delta\omega + \dfrac{m}{n}\Delta\omega$, $l = 1, 2, ..., N$, $\Delta\omega = \dfrac{\omega_u}{N}$; ϕ_{ml} is the random phase

angle distributed uniformly over the interval $[0, 2\pi]$, and the simulated period is given by

$$T_0 = n\frac{2\pi}{\Delta\omega} \tag{13}$$

In the process of simulation, the inflow velocity data in the inlet boundary is made up of a mean wind velocity and a fluctuating wind velocity. The power law describes the mean velocity profile. The horizontal turbulent wind spectrum is adopted in Kaimal's form, and the vertical wind spectrum is in the form presented by Lumley and Panofsky (Han 2007). The coherence function of the wind turbulence adopted is in Davenport's form. The total number of frequency intervals is 1024, and the upper cutoff frequency is 2π. The simulated wind velocity histories are calculated based on

The mean wind velocity:

$$U(z) = U_0(\frac{z}{h_0})^{\alpha} \tag{14}$$

Longitudinal wind spectrum:

$$\frac{nS_u(n)}{u_*^2} = \frac{200f}{(1+50f)^{5/3}} \tag{15}$$

Vertical wind spectrum:

$$\frac{nS_w(n)}{u_*^2} = \frac{6f}{(1+4f)^2} \tag{16}$$

Coherence function:

$$coh_\varepsilon(n) = \exp\left\{-\frac{nC_{x\varepsilon}|x-x'|}{\overline{U}(z)}\right\}(\varepsilon = u, w) \tag{17}$$

where $U(z)$ is the mean wind velocity at the height of z; U_0 is the mean wind velocity at the height of h_0; the power law exponent, α, is 0.16, which is obtained from the wind tunnel test; n is the frequency in Hz; $f = nz/U(z)$ is the dimensionless normalized frequency; $u_* = KU(z)/\ln(\frac{z}{z_0})$ is the shear velocity of the flow, where *K* equals 0.4, z_0 is the roughness height fitted by measured data from the wind tunnel test and is 0.0012 m; $\overline{U}(z)$ is the average of the mean wind speeds at the two positions of x and x', and $C_{xu} = C_{xw} = 16$ are the coefficients related to the wind correlation, i.e., the coherence of the wind turbulence.

The time step in the simulation of the random wind velocity field must be the same as the time step in the simulation of LES. In order to avoid aliasing, the time step Δt has to obey the condition

$$\Delta t \leq \frac{2\pi}{2\omega_u} \tag{18}$$

where ω_u is the upper cut off frequency.

The resolution of the turbulent structures in time is essential for the success of the simulation. The calculation time step in the LES should ensure a Courant-Friendrich-Levy (CFL) number of (Fluent, Education version, V15.0).

$$CFL = \frac{U\Delta t}{\Delta x} \leq 1 \tag{19}$$

MATLAB is adopted to synthesize the turbulent wind velocity data based on the WAWS method considering the power spectrum density and the full spatial correlation. As a matter of fact, the desired value of the distance among points for WAWS would more exactly match the grid points at the inlet boundary of the numerical model. In the current study, the simulated points by the WAWS method are guaranteed to match the grid points in the transverse direction at the inlet boundary. However, in the vertical direction, denser cells near the ground domain are adopted at the inlet boundary, and equal interval simulated points are considered in that place. The generated random wind velocity data of these points which corresponds to the center point of each grid on the inlet boundary is given to the corresponding grids in space, and the linear interpolation method is adopted to assign the wind velocity data to the whole inlet boundary. The assigning process of the random wind velocity data to the inlet boundary of LES is carried out by developing an UDF script, which is implemented into the FLUENT.

3. Validation of the present Inflow turbulence generation approach in LES

To verify the approach presented in this paper, two numerical models are established based on the TJ-2 wind tunnel experiment (Pang, Lin *et al*. 2004). By using the turbulent characteristics obtained from the wind tunnel test, in the first approach the turbulent wind velocity field (TWVF) is generated with the WAWS method as discussed earlier and then assigned to the inlet boundary for the LES. Because no physical elements are used to generate the wind turbulence field, this model is designated as the "empty numerical wind tunnel model (ENWTM)." Since this approach is presented in the present study, it is also referred to as the presented approach. The other one, the "numerical wind tunnel model with spires and roughness elements (NWTM-SR)", is established for the purpose of comparison and verification. In this approach, a uniform wind velocity field (UWVF) is assigned to the inlet boundary for the LES and spires and roughness element. The same ones used in the wind tunnel experiment are used in the numerical wind tunnel to generate the wind turbulence field. The geometries, meshing, calculating parameters, and boundary conditions of these two models are analyzed in the following.

3.1 Geometries and meshing of the models

3.1.1 Empty numerical wind tunnel model

The ENWTM used in the present study has the same dimensions as those of the TJ-2 wind tunnel in Tongji University with the dimensions of 15 m (length) × 3 m (width) × 2.5 m (height). The hexahedral mesh is adopted to ensure the better accuracy, and three kinds of meshing numbers, namely, 0.9 million, 1.8 million, and 4.0 million, have been carried out to test the grid independence. The turbulence intensities of the monitoring point "P2", as shown in Fig. 1, for the three kinds of grids are calculated, and the results are shown in Table 2. It can be seen that the turbulence intensity of the flow field is approaching the stable state when the meshing number is 1.8 million cells. Considering the calculating times and accuracy, the grid model of 1.8 million cells is selected.

Fig. 1 shows the grid of the ENWTM. There are 600 grid points in the longitudinal direction from the inlet to the outlet, 50 grid points in the lateral direction and 60 grid points in the vertical direction. The grid points are distributed uniformly in the longitudinal and lateral directions and distributed unevenly in the vertical direction with the stretching ratio of 1.05 where the grid is denser the closer it gets to the bottom surface.

3.1.2 Numerical wind tunnel model with spires and roughness elements

The NWTM-SR has the same conditions as the wind tunnel experiment (Pang, Lin *et al*. 2004), as shown in Fig. 2. Similarly, the hexahedral mesh is used to simulate spires and roughness elements, and three kinds of grids with the total number of 2.5, 4.5, and 8 million cells are carried out to test the grid independence. Their turbulence intensities are calculated and shown in Table 3. It can be seen that the turbulence intensity of the monitoring point "P2" (as shown in Fig. 2) in the flow field is approaching a stable state when the meshing number is 4.5 million. Considering the calculating times and accuracy, the grid model with 4.5 million cells is selected. Fig. 3 shows the grid of the numerical wind tunnel with spires and roughness elements. There are 800 grid points in the longitudinal direction from the inlet to the outlet, 80 grid points in the lateral direction and 70 grid points in the vertical direction. The grid points in all the three directions are distributed unevenly and clustered near the spires and roughness elements.

Table 2 Independence test of the empty numerical wind tunnel model

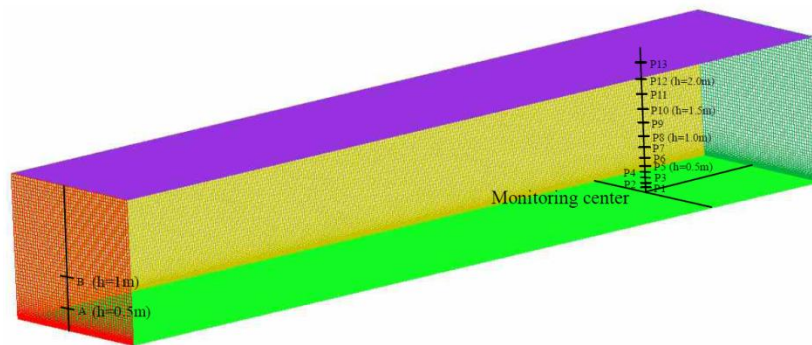| Number of grids	0.9 million	1.8million	4.0 million
Turbulence intensity	8.77%	13.64%	14.13%

Fig. 1 Computation grid of the ENWT model

Table 3 Independence test of the numerical wind tunnel model with spires and roughness element

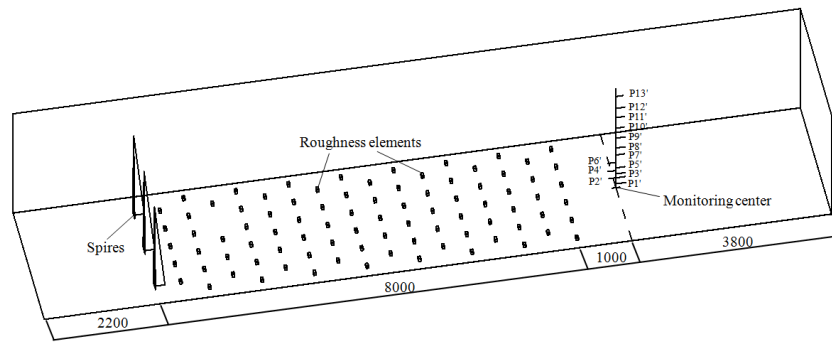| Number of grids	2.6 million	4.5million	8.0 million
Turbulence intensity	9.9%	12.42%	12.49%

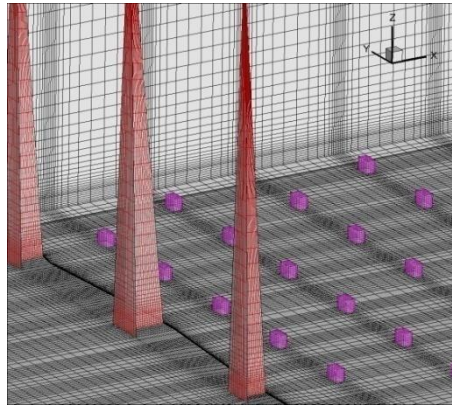Fig. 2 Geometrical dimensions of the NWTM-SR

Fig. 3 Computation grid of the NWTM-SR

3.2 Computational parameters and boundary conditions

The inflow on the inlet boundary for the ENWTM is the random sequence synthesis data generated, which strictly satisfies the measured values from the wind tunnel test. In comparison, the NWTM-SR takes the uniform wind field with the mean wind velocity of 20 m/s on the inlet boundary as shown in Fig. 4. The two models have the same size cells near the ground surface. The same time step of 0.0025 s for the two models, according to the CFL criterion, is adopted for the comparison. To further check the time step independence, three different time steps of 0.001 s, 0.0025 s, and 0.005 s have been carried out. The simulation results show that the results for 0.0025 s are close to those for 0.001 s, which proves that the time step of 0.0025 s is reasonable. The computational parameters and the details of the boundary conditions are listed in Table 4.
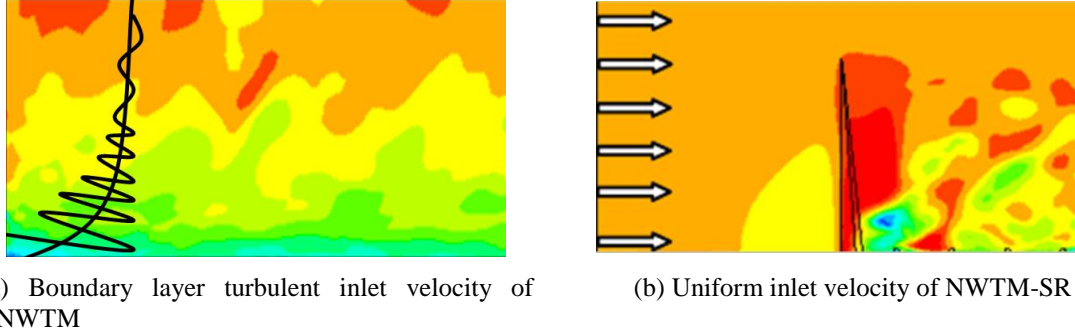
(a) Boundary layer turbulent inlet velocity of ENWTM

(b) Uniform inlet velocity of NWTM-SR

Fig. 4 The inflow on the inlet boundary for ENWTM and NWTM-SR

Table 4 Computational parameters and boundary conditions

Calculate parameters	ENWTM	NWTM-SR
Turbulence model	LES	LES
Grid type	Hexahedron	Hexahedron
Inlet velocity boundary	Turbulent boundary layer	Uniform flow field with U=20m/s
Side of the computational domain	Symmetric	Symmetric
Top of the computational domain	Free slip	Free slip
Bottom of the computational domain	No slip	No slip
Surface of spires roughness element	No slip	Not Applicable
Time step Δt	0.0025s	0.0025s

3.3 Calculation results

The computation is performed by using the supercomputer with 12 CPUs, which can be used in parallel for the whole simulation, with the calculation results as follows.

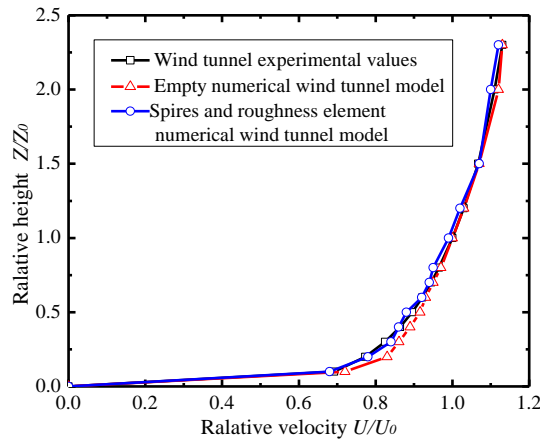### 3.3.1 Analysis of the turbulent wind velocity field at the monitoring center

The wind velocities at the points (P1 to P11 in Fig. 1 and P1' to P11' in Fig. 2) along the "monitoring center" in the vertical direction are monitored. Two minutes averaging time is used to calculating the mean wind profiles and turbulence intensity. The mean wind profile is obtained and compared with the wind tunnel experimental results, as shown in Fig. 5. It can be found that the simulation results of the two models agree well with the wind tunnel experimental results. The mean wind velocity profile of the ENWTM is fitted by the least square method exponentially, and the obtained exponent α is 0.161, which is very close to the experimentally fitted value of 0.160. The turbulence intensity profile as shown in Fig. 6, also agrees well with the wind tunnel test.

Therefore, the presented approach can well generate the target turbulent wind field at the monitoring center, indicating that the wind field on the inlet boundary is accurately generated.

The velocity correlation analysis of points P5 and P10 at the monitoring center for the ENWTM and points P5' and P10' for the NWTM-SR, as shown in Figs. 1 and 2, respectively, is carried out with the results shown in Fig. 7.

As shown in Fig. 7, the correlation functions of the inflow fluctuating wind field declines exponentially, and the declining tendency of the simulation values is in good agreement with that of the targeted theoretical values.

Fig. 8 shows the longitudinal and vertical power spectrums of the ENWTM at point B on the inlet boundary as shown in Fig. 1 and compared them with the Kaimal spectrum. Figs. 9 and 10 show the longitudinal and vertical power spectrums of points P8 and P8' at the monitoring center for the two models along with the Kaimal spectrum and Lumley and Panofsky spectrum.

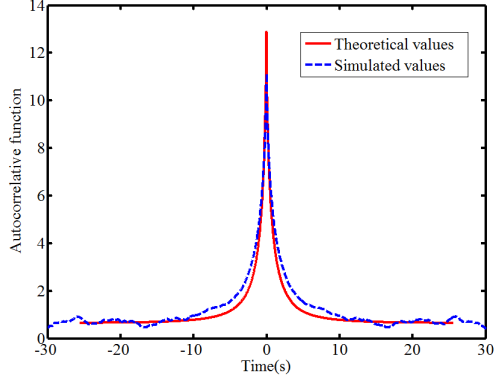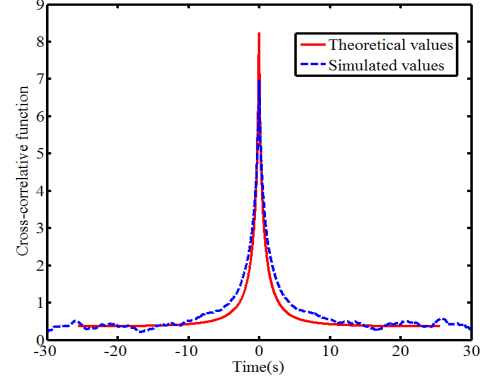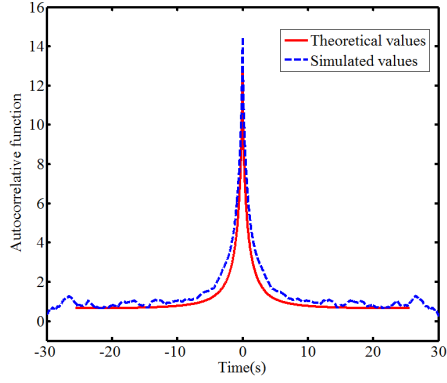Fig. 5 Wind velocity profile at the monitoring center

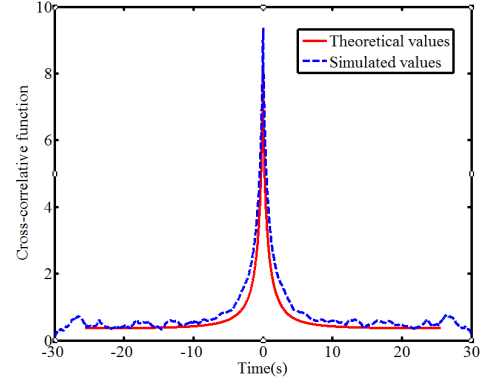Fig. 6 Turbulent intensity profile of longitudinal turbulence at the monitoring center

(a) Autocorrelation function of point P5

(b) Cross-correlation function of point P5 and P10
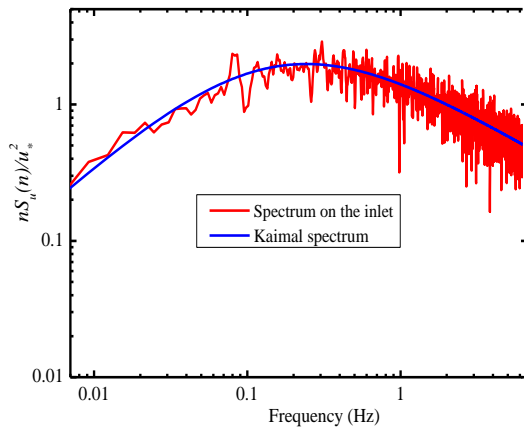

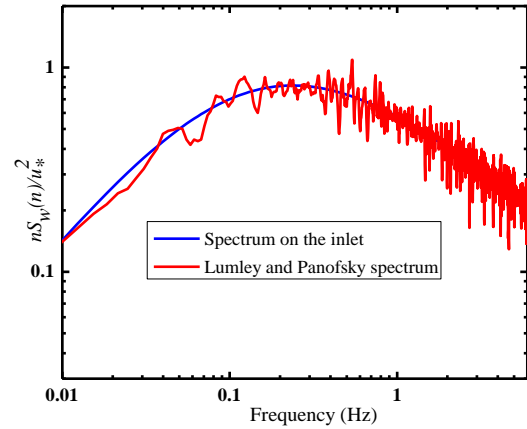(c) Autocorrelation function of point P5'

(d) Cross-correlation function of point P5' and P10'

Fig. 7 Correlation functions of the wind velocity field

(a) Longitudinal power spectrum

(b) Vertical power spectrum

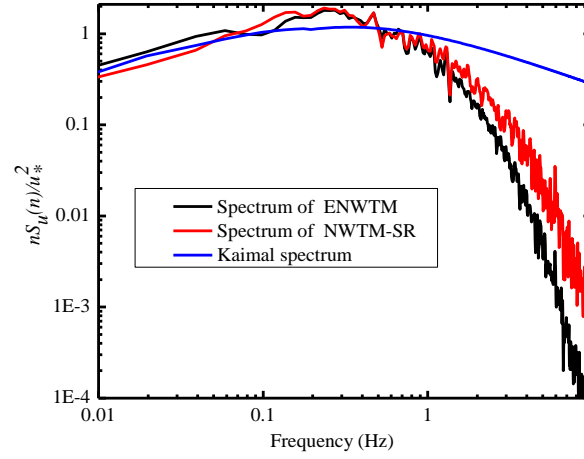Fig. 8 Power spectrum on the inlet boundary

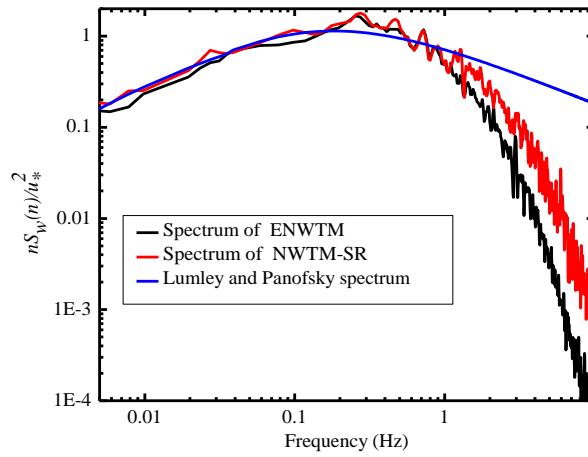Fig. 9 Longitudinal power spectrum at the monitoring center

Fig. 10 Vertical power spectrum of at the monitoring center

Table 5 Comparison of the calculating efficiency for the two models

Model	Number of grid	Calculating time
ENWTM	1.8 million	60 hours
NWTM-SR	4.5 million	124 hours

As shown in Fig. 8, the inlet power spectrum has a good agreement with the target spectrum, i.e. Kaimal spectrum in the whole frequency range. However, as shown in Figs. 9 and 10, there is a reasonable agreement between the power spectral densities of the ENWTM and the NWTM-SR.

However, the difference between these two numerical wind tunnel models becomes larger at higher frequency ranges, and both models are different from the target spectrum in the high frequency range. However, the frequency range of lower than 1 Hz is the range of interest for the present application, especially for wind engineering in urban residential areas. For the frequency < 1 Hz, the power spectral densities of the ENWTM agree basically well with the Kaimal spectrum. It illustrates that the simulated fluctuating wind field in this paper can meet the requirement of the concerned engineering application. For the frequency > 1 Hz, there is a steep drop for the spectrums of LES relative to the Kaimal spectrum. Presently, it is a common phenomenon for the power spectral density of the fluctuating wind velocity to decline in the high frequency range for LES (Noda and Nakayama 2003, Tamura, Tsubokura *et al*. 2003). This is due to the filtering effects of LES calculations and the fact that the energy of the spectrum in the high frequency range is mainly from the contributions of the small vortexes. Ameliorating turbulence models and enhancing the grid resolution can improve this problem. It is noted again that, compared with wind fields for structural analysis, environment wind fields are mainly concerned with the low frequency and low velocity wind.

3.3.2 Analysis of the computational efficiency of the two models

For comparing the computational efficiency of the two numerical models, i.e., ENWTM and NWTM-SR, the grid number and the consuming time for the two models are listed in Table 5.

As shown in Table 5, the grid number and the calculating time of the ENWTM are much less than those of the NWTM-SR, which indicates that the ENWTM is more effective. In addition, the ENWTM that uses the TWVF, when compared to the NWTM-SR, is simpler to carry out and more adaptable to simulate different fluctuating wind fields by adjusting the characteristic parameters of the target fluctuating wind field. Therefore, the ENWTM with the TWVF inlet boundary, instead of using the spires and roughness elements, is presented in order to generate the turbulence wind field in the present study. This approach will be applied in the next case study.

4. Numerical simulation on the wind environment in an urban residential area

4.1 Model of residential neighborhood

A residential neighborhood that is located on the north bank of Tagus River in Lisbon (Ferreira, Sousa *et al*. 2002, Cui, Shi *et al*. 2008) is investigated in this paper. The neighborhood is made up of 7 buildings separated by passageways, as shown in Fig. 11 with the actual dimensions. Due to the large difference between the horizontal and vertical dimensions, the vertical scale is twice as large as the horizontal scale in the east-side view where h1=1.4 m and h2=9.1 m. Ferreira, Sousa *et al*. (2002) carried out wind tunnel experiments and numerical simulations to analyze the interference generated by the two auxiliary structures upon the wind velocity field in the residential neighborhood. In this study, the ENWTM with the TWVF inlet boundary methodology, i.e., the presented methodology, is adopted to analyze the wind environment around the residential neighborhood without the two auxiliary structures, and the simulated results are compared with the experimental results of Ferreira et al.'s study. Eight points are monitored for the evaluation of wind environment along the two passageways L1 and L2, as shown in Fig. 11.
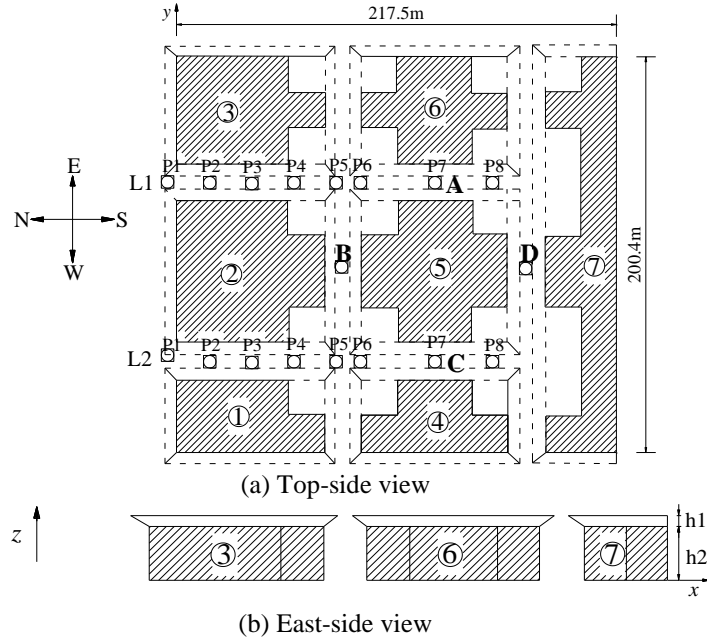
(a) Top-side view

(b) East-side view

Fig. 11 Sketch map of the residential neighborhood under study

4.2 Grid mesh and boundary conditions

To adjust the wind direction easily, a circle calculation domain is adopted in this study, as shown in Fig. 12(a). The calculation domain is divided into 8 parts of equal distance from the external border. Therefore, only small changes are needed to adjust the wind direction. The domain is meshed into hexahedral grids with the O-block method, as shown in Fig. 12(b), the diameter and height of the calculation domain are 900 m and 150 m, respectively, and the total number of the grids is about 4.6 million.

The inflow boundary conditions of the numerical simulation are the same as those of the wind tunnel experiments carried out by Ferreira, Sousa *et al*. (2002). The average wind velocity of the flow is calculated with the formula $u/U_0 = \left(\dfrac{z}{h_0}\right)^{\alpha}$, where h_0 =70 m is the reference height; U_0 =11 m/s is the mean wind velocity at the height of h0; and the exponent α is 0.11. The inlet turbulence intensity obtained from the wind tunnel experiments (Ferreira, Sousa *et al*. 2002), is shown in Fig. 13.

As discussed earlier, in the presented approach, the fluctuating flow information is generated by the WAWS method according to the turbulence intensity and added to the inlet boundary in LES using the ENWTM. To reflect the superiority of the presented approach, for a comparison, the common method in which the velocity, without considering the wind fluctuations in the form of velocity profile, is inputted on the inlet boundary is also adopted here to analyze the wind environment around the residential neighborhood. The numerical simulation on the wind environment around the residential neighborhood is carried out with four cases with different boundary conditions, as shown in Table 6.
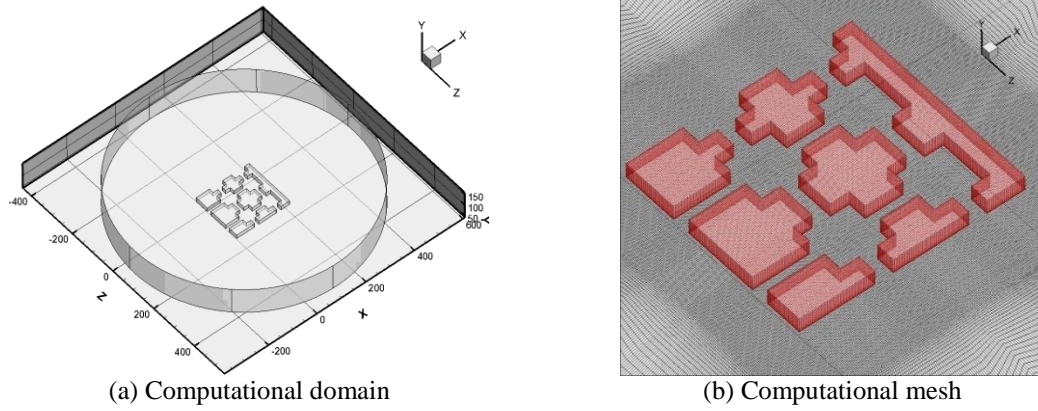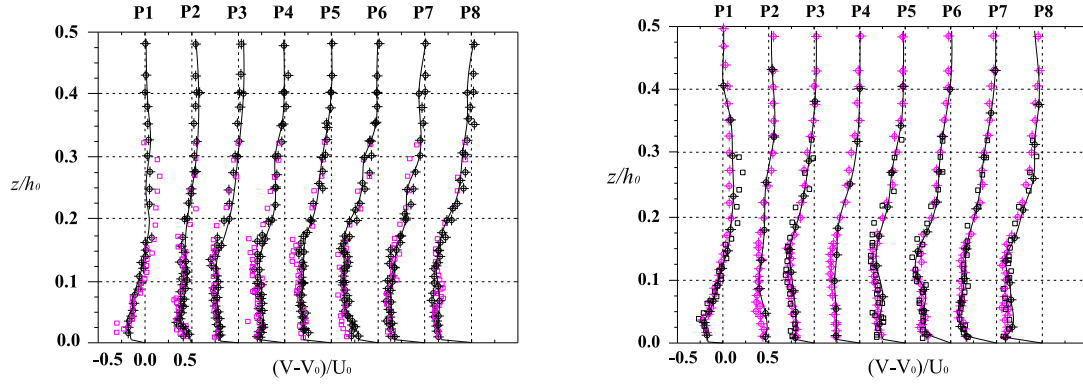
(a) Computational domain

(b) Computational mesh

Fig. 12 Computational domain and mesh

Table 6 Simulation cases

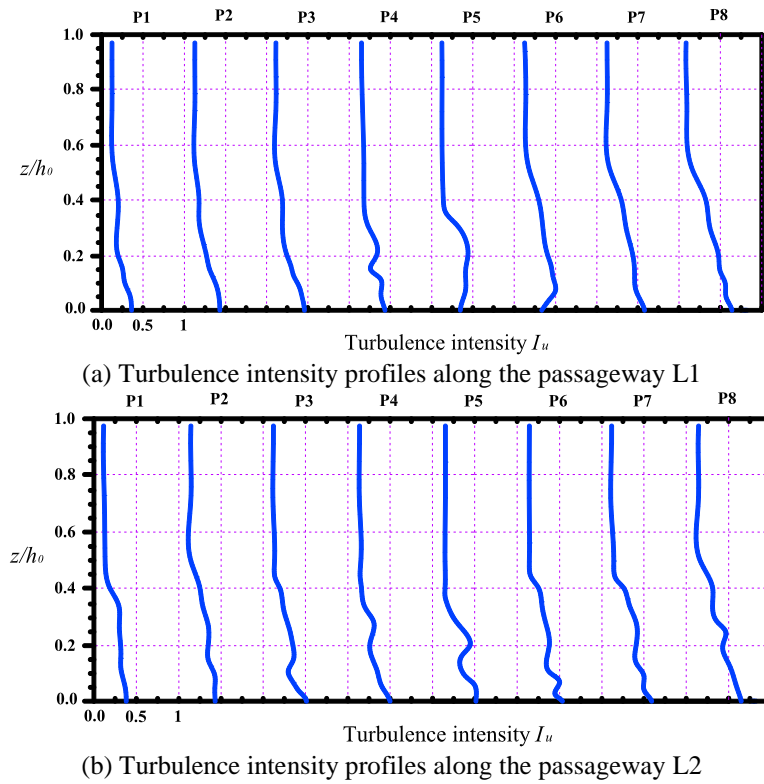| Cases	Wind Direction	The inputting method of the wind field
1	North	The presented methodology
2	North	The common method without inlet fluctuations
3	Northeast	The presented methodology
4	Northwest	The presented methodology

4.3 Calculating results

For Case 1, the mean wind velocity profiles of points P1-P8 along the passageways L1 and L2 are obtained and compared with the wind tunnel experimental results measured by Ferreira, Sousa *et al.* (2002), as shown in Fig. 14, where V is the wind velocity magnitude, V_0 is the inlet flow conditions at the same level, and the velocity difference is normalized by the wind velocity U_0. The mean wind velocity profiles at different positions in the residential neighborhood are well reflected in these figures.

From Fig. 14, it can be observed that the simulation results in this study agree well with the experimental results measured by Ferreira, Sousa *et al.* (2002) for passageways L1 and L2. The buildings in the residential neighborhood have obvious influence on the mean wind velocity profiles, especially for the near ground. The mean wind velocity declines obviously near the ground. The higher the height is, the smaller the decline tendency of the mean wind velocity is. As the height is twice or more the height of the buildings, the difference between the mean wind velocity of the monitoring point and the inlet flow conditions at the same level is small. The mean wind velocity along the horizontal direction declines as well due to the influence of the friction of the buildings. Meanwhile, the longer the horizontal distance from the inlet is, the larger the influence on the average wind velocity is.

(a) Velocity profiles along the passageways L1   (b) Velocity profiles along the passageways L2

("□" stands for the measured value of 7-hole probe in the wind tunnel experiment；"⊕" is the

measured value of hot-wire anemometer" ——— "is the simulated wind velocity)

Fig. 14 Velocity profiles at the monitoring points along the passageways

(a) Turbulence intensity profiles along the passageway L1

(b) Turbulence intensity profiles along the passageway L2

Fig. 15 Turbulence intensity profiles at the monitoring points along the passageways

(a) Point A   (b) Point B
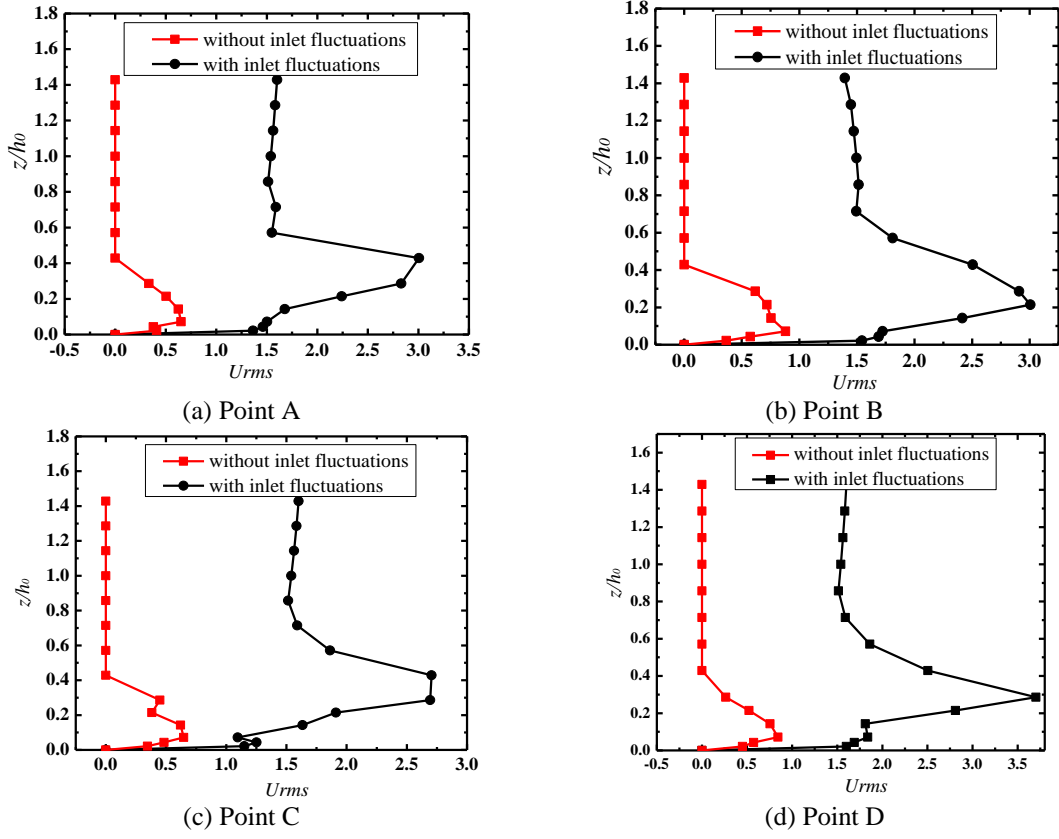
(c) Point C   (d) Point D

Fig. 16 Velocity root mean square

Fig. 15 presents the turbulence intensity profiles at the monitoring points along the passageways L1 and L2 for Case 1. From Fig. 15, it can be observed that the turbulence intensities increase obviously near the ground. When the height is twice or more the height of the buildings, the turbulence intensity of the monitoring points is the same as that of the inlet level. Meanwhile, it can be found that the turbulence intensities are also influenced by the horizontal distance from the inlet, and the turbulence intensity near the ground increases with the increase of the distance.

In order to understand the influence of the inlet fluctuations, the root mean square (RMS) values of the velocities simulated at points A~ D for Case 1 and Case 2 are compared and shown in Fig. 16. It is clearly found that the RMS values of velocities for Case 1 (with the inlet fluctuation) are larger than those for Case 2 (without the inlet fluctuation) on the whole. The RMS values of velocities increase at first, then decrease, and finally trend to be a constant value with the dimensionless height z/h_0. It can be seen from Fig. 16(a) that the value trends to be about 1.5 m/s when z/h_0 is larger than 0.6 for Case 1, but is close to zero when z/h_0 is larger than 0.4 for Case 2. Similar change laws can be found in Figs. 16(b)-16(d). From the above analysis, it is indicated that the turbulence in the flow field for Case 1 is better developed than that for Case 2. Therefore, the inclusion of the inlet fluctuations is very important for generating a reasonable turbulent wind field, which in turn plays a significant role in the process of contaminant dispersion among groups of buildings.
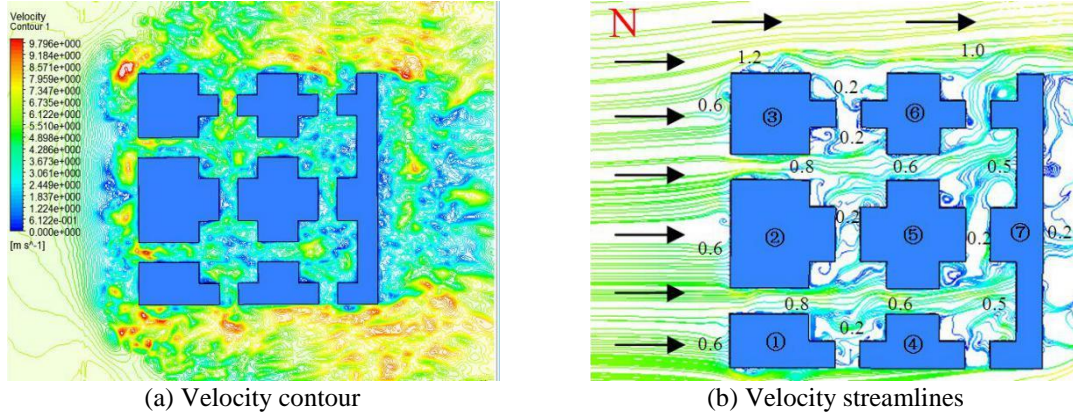
(a) Velocity contour   (b) Velocity streamlines

Fig. 17 Velocity contour and velocity streamlines with wind from north (Case 1)

(a) Velocity contour   (b) Velocity streamlines
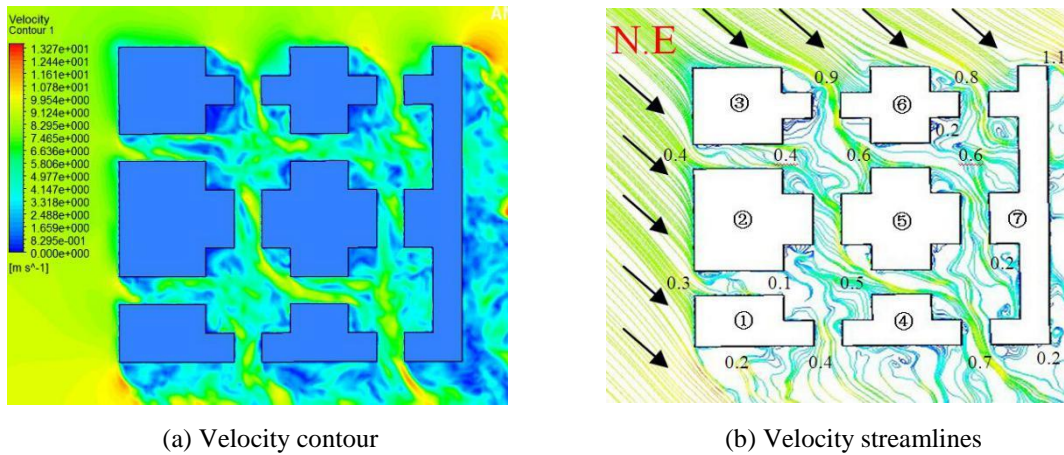
Fig. 18 Velocity contour and velocity streamlines with wind from northeast (Case 3)

The average wind velocity in the residential neighborhood must be kept in a certain range, i.e., it cannot be too high or too low. A wind velocity that is too high will make pedestrians uncomfortable while a wind velocity that is too low will impede ventilation resulting in the accumulation of pollutants and thus influence people's health. It is pointed out in the concerned code (JGJT229-2010) that when the average wind velocity reaches 5m/s, people will feel uncomfortable. In order to analyze the wind environment at the pedestrian level in detail, the velocity contour and the velocity streamlines of the wind field around the residential neighborhood at the height of 1.5 m with the wind directions from the north, northeast, and northwest are presented in Figs. 17-19, for Case 1, Case 3, and Case 4, respectively. As shown in Fig. 17(a), the high wind velocities appear near the left end of the passageways L1 and L2 due to the channeling effect induced by the decreasing of flow section. Meanwhile, the wind velocities decline from the

left to the right along the passageways L1 and L2 due to the blocking effect of the Building 7. The velocities in the leeward region are relatively small, and there are obvious vortexes around the corners due to the flow separation. As shown in Figs. 18(a) and 19(a), it is obvious that high wind velocities appear at the windward corners of the buildings and at the passageways along the mainstream direction of flow for the same reason, i.e. the channeling effect. Meanwhile, there are vortexes in the leeward corners where velocities are obviously lower than those of the other regions.

Wind velocity ratio is adopted in this paper and defined as $R_i = U_i / U_0(z)$, where U_i is the average wind velocity at the position of i, and $U_0(z)$ is the inflow average wind velocity at the same height. R_i is called the acceleration factor of wind velocity, which illustrates the velocity changes resulting from the impeded wind field within the neighborhood. In Fig. 17(b), the maximum wind velocity ratio of 1.2 is found at the northwest corner of Building 3, and the wind velocity ratio value of 0.8 is found at the entrance region of passageways L1 and L2. Due to the blocking effect of Building 7, the wind velocity ratio value declines gradually along the passageways L1 and L2, and the minimum wind velocity ratio value of 0.2 is found in the corridors between the buildings and on the rear side of Building 7. As shown in Fig. 18(b), the maximum wind velocity ratio value of 1.1 is found in the northeast corner of Building 7, and the minimum wind velocity ratio value of 0.2 is found in the southeast corner of Building 7. As shown in Fig. 19(b), the maximum wind velocity ratio value of 1.2 is found in the southeast corner of Building 7, and the minimum wind velocity ratio value is found in the northeast corner of Building 7.

From the above results, it can be observed that strong wind velocities, which may occur at the passageways along the mainstream direction of flow, may affect the comfort of pedestrians at the ventilation corridor in the residential neighborhood. Meanwhile, the pollutants cannot be spread well at the leeward corners of buildings where the small wind velocities and vortexes may appear.

(a) Velocity contour   (b) Velocity streamlines
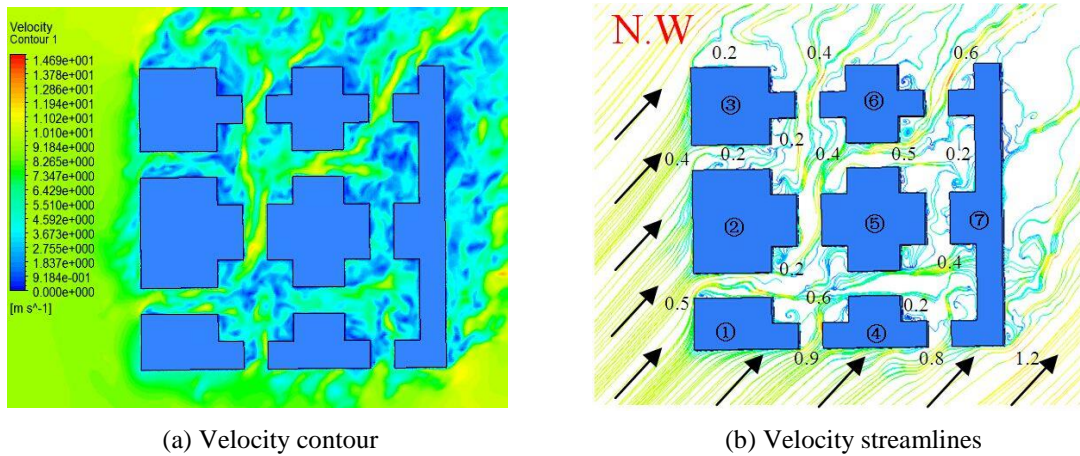
Fig. 19 Velocity contour and velocity streamlines with wind from northwest (Case 4)
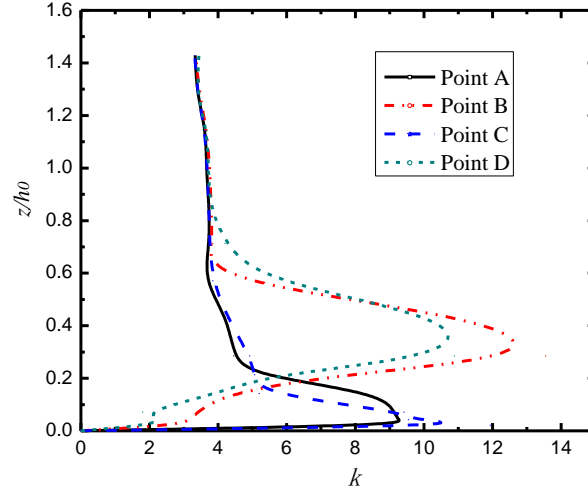
Fig. 20 Profile of turbulent kinetic energy (Case 1)

The turbulence intensity is the other factor that can affect the comfort of pedestrians in the residential neighborhood. The distribution of the turbulent kinetic energy (TKE) along the height can reflect the spatial variation of the turbulence intensity. To facilitate the understanding of the distribution of the TKE around the residential neighborhood, the profiles of the TKE at the points A-D (defined in Fig. 11) for Case 1 are investigated and shown in Fig. 20. As shown in Fig. 20, the TKE increases at first, then decreases with the dimensionless height z/h_0, and finally trends to be a constant value (i.e., the TKE of the free flow). For points A and C at the passageways L1 and L2, the maximum values of TKEs occur at the height of 1.5 m (i.e., z/h_0 is 0.021), which is about the pedestrian level height, and the values gradually decrease with the height and also trend to be close to the TKE of the free flow at about the height of 18 m. For points B and D at the passageways, which are perpendicular to the direction of the incoming flow, the maximum values of TKEs occurred at about the height of 20 m (i.e., z/h_0 is about 0.3) on the building tops in the strong shear region, and the values gradually decrease with the height and then trend to be close to the TKE of the free flow at about the height of 56 m. The above analysis indicates that the comfort degree of pedestrians at the passageways L1 and L2 is lower than that at other positions not only because of the higher average wind velocity, but also because of the higher TKE at the pedestrian level at these passageways.

5. Conclusions

An inflow turbulence generating approach is presented in the present study based on the weighted amplitude wave superposition (WAWS) method, which can generate a fluctuating wind flow field satisfying any desired target spectrum by the technique of WAWS. Then, the presented approach is successfully applied to simulate the wind environment around a real residential neighborhood, and the numerical results are compared with the wind tunnel experimental results.

Based on the analysis results, following conclusions can be drawn:

• The inflow turbulent flow field with the prescribed spectra can be well generated using the presented approach. By the comparison of the numerical results with the wind tunnel experimental results, it is revealed that the inflow turbulence generating approach based on the weighted amplitude wave superposition (WAWS) method is accurate and can satisfy the requirement of the engineering application. Then, by comparing the calculating efficiency of the presented approach with that of the NWTM-SR approach, it is found that the presented approach is more efficient and adaptable.

• The mean wind velocity and turbulence intensity profiles at different positions in the residential neighborhood are investigated and validated by comparing them with the experimental results. The results show that the mean wind velocity declines while turbulence intensity increases obviously on the near ground. When the height is twice or more the height of the buildings, the mean wind velocity and turbulence intensity of the monitoring point are essentially the same as that of the inlet flow at the same level. The horizontal distance from the inlet also influences the average wind velocity and turbulence intensity.

• By comparing the root mean square (RMS) values of the velocities at the points in the residential neighborhood, it is observed that the inclusion of the inlet fluctuations is very important for generating a reasonable turbulent wind field, which in turn plays a significant role in the process of contaminant dispersion among groups of buildings.

• By the analysis of the average wind velocity at the height of 1.5 m and the TKE around the residential neighborhood, it is observed that the stronger wind velocities and the higher TKEs occur at the passageways along the mainstream direction of flow which may affect the comfort of people at the pedestrian level in the residential neighborhood. The small wind velocities and vortexes appear at the leeward corners of buildings, which may affect the spreading of pollutants.

Acknowledgements

References

ANSYS® Academic Research, Release 15.0.

Britter R.E. and Hanna S.R. (2003), "Flow and dispersion in urban area", *Annu. Rev. Fluid. Mech.*, **35**, 469-495.

Castro H.G. and Paz R.R. (2012), "A time and space correlated turbulence synthesis method for large eddy simulations", *J. Comput. Phys.*, **235**, 742-763.

Chen, Z., Han, Y., Hua, X. and Luo, Y. (2009), "Investigation on influence factors of buffeting response of bridges and its aeroelastic model verification for Xiaoguan Bridge", *Eng. Struct.*, **31**, 417-431.

Chung Y.M. and Sung H.J. (1997), "Comparative study of inflow conditions for spatially evolving simulation", *AIAA J.*, **35**(2), 269-274.

Cui G.X., Zhang Z.X. and Xu C.X. (2013), "Research advances in large eddy simulation of urban

atmospheric environment", *J. Adv. Mech.*, **43**(3), 295-328. (in Chinese)

Cui, G.X., Shi, R.F., Wang, Z.S, Xu, C.X. and Zhang, Z.X. (2008), "Large eddy simulation of urban micro-atmospheric environment", *J. Sci. china*, **38**(6), 626-636. (in Chinese)

Deodatis, G. (1996), "Simulation of ergodic multivariate stochastic processes engineering mechanics", *J. Eng. Mec*h., **122**(8), 778-787.

Di Paola, M. (1998), "Digital simulation of wind field velocity", *J. Wind. Eng. Ind. Aerod.*, **74-76**, 91-109.

Ding, Q., Zhu, L. and Xiang, H. (2006), "Simulation of stationary Gaussian stochastic wind velocity field", *Wind Struct.*, **9**(3), 231-243.

Ferreira, A.D., Sousa, A.C.M. and Viegas, D.X. (2002), "Prediction of building interference effects on pedestrian level comfort", *J. Wind Eng. Ind. Aerod.*, **90**, 305-319.

Fureby, C. (1996), "On subgrid scale modeling in large eddy simulations of compressible fluid flow", *J. Phys. Fluids*, **8**, 1301-1311.

Germano, M., Piomelli, U., Moin, P. and Cabot, W.H. (1991), "A dynamics subgrid-scale eddy viscosity model", *J. Phys. Fluids*, **3**(7), 1760-1765.

Gousseau, P., Blocken, B. and van Heijst, G.J.F. (2012), "CFD simulation of pollutant dispersion around isolated buildings: On the role of convective and turbulent mass fluxes in the prediction accuracy", *J. Hazardous Mater.*, **194**, 422-434.

Han, Y. (2007), "Study on Complex Aerodynamic Admittance Functions and Refined Analysis of Buffeting Response of Bridge", Hunan university doctoral dissertation. (in Chinese)

Hanna, S.R., Tehranian, S., Carissimo, B., MacDonald, R.W. and Lohner, R. (2002), "Comparisons of model simulations with observations of mean flow and turbulence within simple obstacle arrays", *J. Atmosph. Environ.*, **36**, 5067-5079.

Hemon, P. and Santi, F. (2007), "Simulation of a spatially correlated turbulent velocity field using biorthogonal decomposition", *J. Wind Eng. Ind. Aerod.*, **95**(1), 21-29.

Hoshiya, M. (1972), "Simulation of multi-correlated random processes and application to structural vibration problems", *Proceedings of JSCE*, **204**, 121-128.

Huang, S.H., Li, Q.S. and Wu, J.R. (2010), "A general inflow turbulence generator for large eddy simulation", *J .Wind Eng. Ind. Aerod.*, **98**, 600-617.

Iwatani, Y. (1982), "Simulation of multidimensional wind fluctuations having any arbitrary power spectra and cross spectra", *J. Wind Eng. Jpn.*, **11**, 5-18.

Jiang, G., Yoshie, R., Shirasawa, T. and Jin, X. (2012), "Inflow turbulence generation for large eddy simulation in non-isothermal boundary layers", J. *Wind Eng. Ind. Aerod.*, **104**(106), 369-378.

Jiang, W.M. and Miao, S.G. (2004), "30 years review and perspective of the research on the large eddy simulation and atmospheric boundary layer", *J. Adv. Natural Sci.*, **14**, 11-19. (in Chinese)

Kataoka, H. and Mizuno, M. (2002), "Numerical flow computation around aeroelastic 3D square cylinder using inflow turbulence", *Wind Struct.*, **5**(2-4), 379-392.

Keating, A., Piomelli, U., Balaras, E. and Kaltenbach, H.J. (2004), "A priori and a posteriori tests of inflow conditions for large-eddy simulation", *J. Phys. Fluids*, **16**, 46-96.

Kondo, H., Asahi, K., Tomizuka, T. and Suzuki, M. (2006), "Numerical analysis of diffusion around a suspended expressway by a multi-scale CFD model", *J. Atmosph. Environ.*, **40**, 2852-2859.

Kondo, K., Murakami, S. and Mochida, A.,(1997), "Generation of velocity fluctuations for inflow boundary condition of LES", *J. Wind Eng. Ind. Aerod.*, **67-68**, 51-64.

Kraichnan, R.H. (1970), "Diffusion by a random velocity field", *J. Phys. Fluids*, **13**(1), 22-31.

Liu, Z., Ishihara, T., He, X. and Niu, H. (2016b), "LES study on the turbulent flow fields over complex terrain covered by vegetation canopy", *J .Wind Eng. Ind. Aerod.*, **155**, 60-73.

Liu, Z., Ishihara, T., Tanaka, T. and He, X. (2016a), "LES study of turbulent flow fields over a smooth 3-D hill and a smooth 2-D ridge", *J .Wind Eng. Ind. Aerod.*, **153**, 1-12.

Lund, T.S., Wu, X.H. and Squires, K.D. (1998), "Generation of turbulent inflow data for spatially-developing boundary layer simulations", *J. Comput. Phys.*, **140**, 233-258.

Mann, J. (1998), "Wind field simulation", *Probabilist. Eng Mech.*, **13**, 269-282.

Maruyama, T. and Morikawa, H. (1994), "Numerical simulation of wind fluctuation conditioned by

experimental data in turbulent boundary layer", *Proceedings of the 13th Symposium on Wind Engineering*.

Mathey, F., Cokljat, D., Bertoglio, J.P. and Sergent, E. (2006), "Assessment of the vortex method for large eddy simulation inlet conditions", *Prog. Comput. Fluid Dy.*, **6**, 59-67.

Ministry of Housing and Urban-Rural Development (MOHUR), "Code for green design of civil buildings", JGJT229-2010, China.

Noda, H. and Nakayama, A. (2003), "Reproducibility of flow past two-dimensional rectangular cylinders in a homogeneous turbulent flow by LES", *J. Wind Eng. Ind. Aerod.*, **91**, 265-278

Nozawa, K. and Tamura, T. (2002), "Large eddy simulation of the flow around a low-rise building immersed in a rough-wall turbulent boundary layer", *J. Wind Eng. Ind. Aerod.*, **90**, 1151-1162.

Pang, J.B. and Lin, Z.X. and Chen, Y. (2004), "Discussion on the simulation of atmospheric boundary layer with spires and roughness elements in wind tunnels", *Exp. Meas. Fluid Mech.*, **18**(2), 32-37. (in Chinese)

Shinozuka, M., Yun, C.B. and Seya, H. (1990). "Stochastic methods in wind engineering", *J. Wind. Eng. Ind. Aerod.*, **36**(90), 829-843.

Smirnov, R., Shi, S. and Celik, I. (2001), "Random flow generation technique for large eddy simulations and particle-dynamics modeling", *J. Fluid. Eng. -T ASME*, **123**, 359-371.

Tabor, G.R and Baha-Ahmadi, M.H. (2010), "Inlet conditions for large eddy simulation: a review", *Comput. Fluids*, **39**(4), 553-567.

Tamura, T. (2000), "Towards practical use of LES in wind engineering", *J. Wind Eng. Ind. Aerod.*, **96** (10-11), 1451-1471.

Tamura, T., Tsubokura, M., Cao, S. and Furusawa, T. (2003), "LES of spatially-developing stable/unstable stratified turbulent boundary layers", *Direct Large-Eddy Simul.*, **5**, 65-66.

Tominaga, Y., Mochida, A., Murakami, S. and Sawaki, S. (2008), "Comparison of various revised k- models and LES applied to flow around a high-rise building model with 1:1:2 shape placed within the surface boundary layer", *J. Wind Eng. Ind. Aerod.*, **96**, 389-411.

Wang, D., Yu, X.J., Zhou, Y. and Tse, K.T. (2015), "A combination method to generate fluctuating boundary conditions for large eddy simulation", *Wind Struct.*, **20**(4), 579-607.

Xie, Z.T. and Castro, I.P. (2008), "Efficient generation of inflow conditions for large eddy simulation of street-scale flows", *Flow Turbul. Combust.*, **81**, 449-470.

Yan, B.W. and Li, Q.S. (2015), "Inflow turbulence generation methods with large eddy simulation for wind effects on tall buildings", *Comput. Fluids*, **116**, 158-175.

Yu, R.X. and Bai, X.S. (2014), "A fully divergence-free method for generation of inhomogeneous and anisotropic turbulence with large spatial variation", *J. Comput Phys.*, **256**: 234-253.

CC